Monitoring lipid phase transition temperatures using fluorescent probes and temperature-dependent fluorescence spectroscopy

Zlatko Brkljača[a, 1,+], Mirsada Ćehić[b,+], Tomislav Portada[a], Marija Butumović[c], Danijela Bakarić[a,*], Ivo Crnolatac[a,*]

[a] Division for Organic Chemistry and Biochemistry, Ruđer Bošković Institute, Bijenička 54, 10000 Zagreb, Croatia

[b] Division for Physical Chemistry, Ruđer Bošković Institute, Bijenička 54, 10000 Zagreb, Croatia

[c] Division of Analytical Chemistry, Department of Chemistry, Faculty of Science, University of Zagreb, Horvatovac 102a, 10000 Zagreb, Croatia

[+]equal contribution

[*]Corresponding authors

Abstract

The response of fluorescent dyes incorporated in multilamellar liposomes was evaluated for their applicability in monitoring thermal-induced changes in liposomes. Five fluorescent probes, diverse in polarity, lipophilicity, and consequently their position within the lipid multibilayers constituted from 1,2-dipalmitoyl-*sn*-glycero-3-phosphocholine (DPPC), were used to record temperature-dependent fluorescence spectra of the liposomal suspensions. The responses of the dyes were analysed in a multivariate fashion to determine pre- and main phase transition temperatures of DPPC. Laurdan® and 1-chloro-9,10-bis(phenylethynyl)-anthracene register both phase transitions, while 9,10-diphenylanthracene and 9,10-bis(phenylethynyl)-anthracene report only pretransition. According to the differential scanning calorimetry measurements, all suspensions display both phase transitions that resemble DSC curve of pure DPPC. The positions of the dyes within the bilayers were determined by molecular dynamics simulations.

[1] Present address: Selvita d.o.o. Prilaz baruna Filipovića 29, 10000 Zagreb, Croatia

Keywords: 1,2-Dipalmitoyl-*sn*-glycero-3-phosphocholine (DPPC); Fluorescent dyes, Differential scanning calorimetry (DSC); Fluorescence spectroscopy; Multivariate curve analysis, molecular dynamics simulations

1. Introduction

The interaction with cellular membranes or membrane models is one of the most studied topics in biomedical research.[1,2,3] Transport through the membranes is always a part of the drug delivery studies. Furthermore, the membrane itself, more specifically, the membrane proteins, are frequently the drug targets since there are numerous diseases related to the function of membrane proteins. Even if the interaction with the targeted proteins is well described, the interaction with the surrounding membrane lipids should be evaluated as well. Steady-state or time-resolved fluorescence spectroscopy and microscopy are among the most widely used techniques for visualisation and evaluation of membrane integrity, structure, organization and dynamics.[4] To efficiently monitor liposome integrity, the fluorescent probes should not interfere with the assembly, structure or dynamics while being embedded in the bilayer and reporting minute changes in the environment.[5]

Liposomes constituted from 1,2-dipalmitoyl-*sn*-glycero-3-phosphocholine (DPPC) lipids, formed by self-assembly of DPPC into lipid bilayers, are frequently used membrane models for studying membrane interactions. The long lipid aliphatic chains of DPPC provide sufficient hydrophobic interactions for the reproducible and problem-free formation of liposomes, while the polar headgroups of DPPC ensure stable equilibrium in a water-based environment. Upon heating, the transformation of DPPC from the gel ($L_{\beta'}$) to fluid (L_{α}) is preceded by the pretransition from gel to ripple phase ($P_{\beta'}$), which manifests itself with periodic ripples on the membrane surface, where more prominent hydration occurs.[6, 7] The temperature interval between pre- and main transition depends on the lipid chain length, with DPPC this gap is about 8 °C.[8] $L/P_{\beta'} \rightarrow L_{\alpha}$ phase transition is a highly energetic, cooperative and fast process, characterized by the disruption of hydrogen bonds and van der Waals interactions, whereas the pretransition is much less energetic and cooperative.

Thermal properties of lipid (multi)bilayers can be examined by monitoring the temperature-dependent behaviour of fluorescent probes incorporated at various depths in the bilayer[9,10]. As lipids undergo melting, the environment of the fluorescent probe changes, which is reflected in the change in its response. In the case of Laurdan, a shift in the wavelength maximum, accompanied by the intensity change, is observed[11], while in some pyrrolo-quinoline

fluorescent probes (LD-473 and LD-423), only the signal intensity in the fluorescence spectrum changes[12]. To the best of our knowledge, the responses of the fluorescent probes to the change in lipid bilayer thermal behaviour and the consequent indirect characterisation of phase transitions are rather scarcely documented.

To address the above issue, we examined the changes in thermal properties of DPPC multibilayers in the presence of several hydrophobic and one relative amphiphilic fluorescent probes: Laurdan, DPA, BPEA, Cl-BPEA, Rhodamine B (Fig. 1). 6-lauryl-2-dimethylamino-naphthalene (Laurdan; L)[13] is one of the most frequently used membrane probes. The naphthalene fluorophore offers relatively high fluorescence quantum yield, while the lauryl moiety ensures hydrophobicity and similarity with the lipid part of phospholipids.[14] 9,10-diphenylanthracene (DPA); 9,10-bis(phenylethynyl)-anthracene (BPEA) and 1-chloro-9,10-bis(phenylethynyl)-anthracene (Cl-BPEA) are hydrophobic fluorophores exhibiting high fluorescence quantum yield.[15] In comparison with probes above, Rhodamine B (R) is less hydrophobic and offers more insight into liposome partitioning of more polar, water-soluble probes.[16] Thermal properties of DPPC multilamellar liposomes in the presence of listed fluorescent probes are examined using differential scanning calorimetry (DSC), a technique standardly used in the characterisation of lipid bilayer thermodynamic properties.[17] and temperature-dependent fluorescence spectroscopy to unravel the changes in fluorescent probes signals as DPPC undergoes phase transitions. Temperature-dependent fluorescent spectra are analysed with multivariate curve analysis that demonstrated the success in displaying the phase transition temperature even from temperature-dependent UV/Vis spectra of blank DPPC liposomes[18]. Our experimental data are supported with MD calculations that provide an insight into the location of a particular probe at a carefully selected temperature in the gel and fluid phase, respectively.

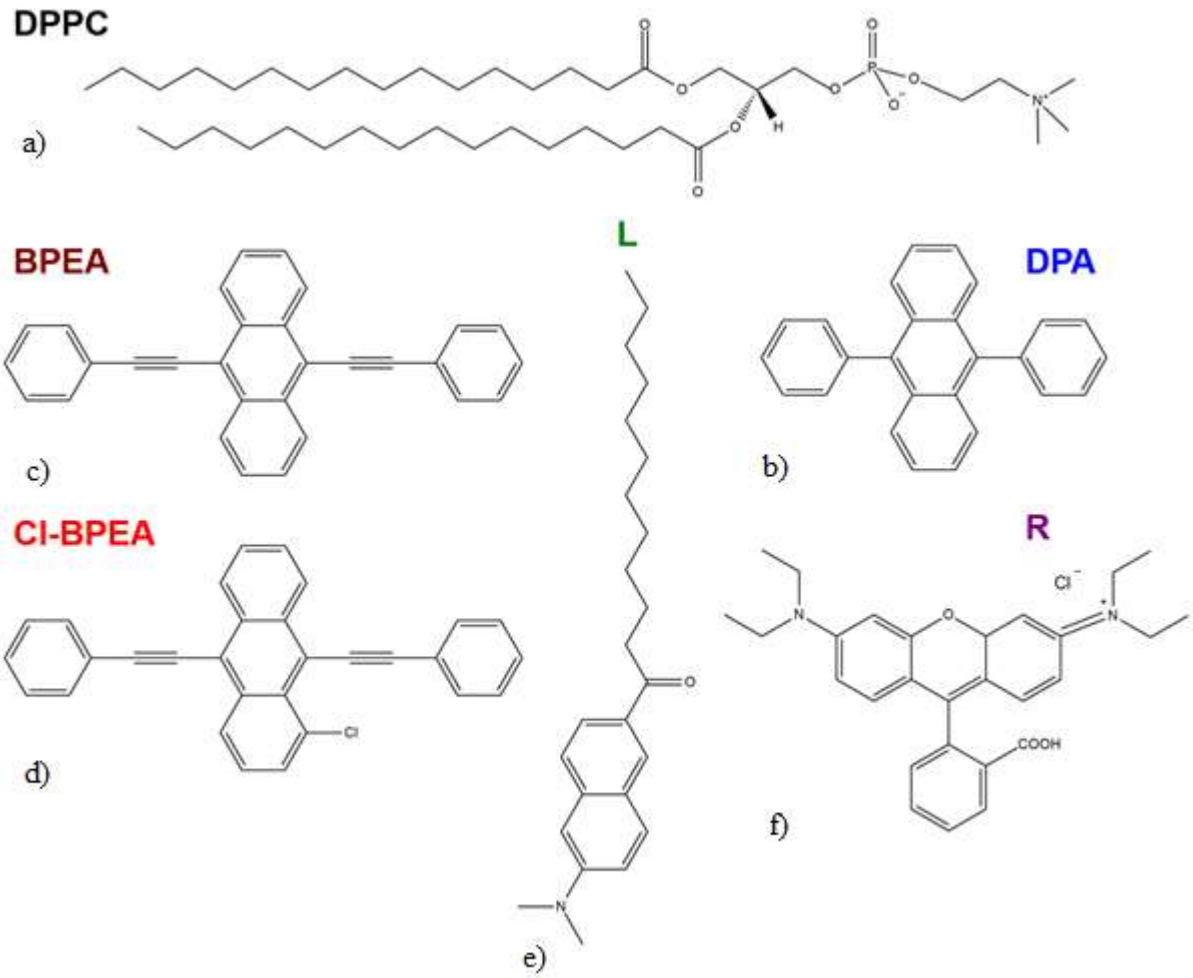

Fig. 1. Structural formulas of a) DPPC and fluorescent probes: b) DPA, c) BPEA, d) Cl-BPEA, e) Laurdan (L) and f) Rhodamine B (R).

2. Experimental

2.1 Chemicals and suspensions preparations

1,2-Dipalmitoyl-*sn*-glycero-3-phosphocholine (DPPC; Mr = 734.04, white powder, purity ≥ 99 %) and laurdan (L; white powder, Mr = 353.54, purity ≥ 98 %) were purchased from Avanti Polar Lipids, rhodamine B (R; dark green powder, Mr = 479.01) from Fluka . DPA (pale yellow powder, Mr = 330.42), BPEA (orange powder, Mr = 378.50) and Cl-BPEA (orange powder, Mr = 412.90) were synthesized according to the published protocols[19,20] FTIR and NMR (^{1}H and ^{13}C) spectra of here prepared compounds show excellent agreement with their reference spectra[21,22,23,24] (details are presented in Supporting Information, section S1). Phosphate buffer of ionic strength I = 100 mM and pH 7.3 in milli-Q water was prepared from Na_2HPO_4 (white powder, AlphaAeEsar, p. a. grade) and NaH_2PO_4 (white powder, Fluka, p. a. grade).

Chloroform ($CHCl_3$; colorless liquid), ethanol (EtOH; colorless liquid) and hexane (HEX; colorless liquid) were purchased from Gram-Mol (p. a., spectroscopic grade and HPLC grade, respectively). All chemicals were used as received.

Stock solution of investigated fluorescent probes were prepared in $CHCl_3$ (DPA, BPEA, Cl-BPEA, L), EtOH (DPA, BPEA, Cl-BPEA) and HEX (DPA, BPEA, Cl-BPEA) so theirs concentrations were 1 mM in $CHCl_3$, ~ $1 \cdot 10^{-4}$ M in EtOH and ~ $1 \cdot 10^{-4}$ M in HEX, respectively, whereas stock solution of R in EtOH was c = 1 mM (L is not soluble in EtOH and HEX and R is not soluble in $CHCl_3$ and HEX).

Stock solutions of DPPC in the absence (colorless) and in the presence of DPA (colorless) / BPEA (green) / Cl-BPEA (orange-green) / L (green) in $CHCl_3$ as well as in the presence of R in EtOH (pink) were prepared as follows: i) 300 mg of DPPC was dissolved in 6 ml of $CHCl_3$; ii) 1 ml of the stock solution was distributed in 6 round bottom flasks so that each flask contained 50 mg of DPPC; iii) in five flasks stock solutions of fluorescent probes were added so their mole ratio in DPPC was x ~ 2 % ml (to meet this mole ratio, 920 μl of stock solution of DPA (in $CHCl_3$), 1315 μl of stock solution of BPEA (in $CHCl_3$), 1434 μl of stock solution of Cl-BPEA (in $CHCl_3$), 1223 μl of stock solution of L (in $CHCl_3$) and 1665 μl of stock solution (in EtOH) of R, respectively, was added). The remained sixth flask contained only DPPC. In all six samples $CHCl_3$ was removed from the flask on rotary evaporator and the obtained film was subsequently dried under Ar stream. Afterwards, multilamellar DPPC liposomes were prepared by suspending the corresponding films in 1 ml of a phosphate buffer (pH 7.3). The samples were vortexed and alternated between a hot and ice H_2O bath. In each of these three steps the sample was held for about one minute. The cycle of vortexing and heating and cooling of the sample were repeated for five times. These suspensions were further used as stocks for fluorimetric and DSC measurements.

2.2 Fluorescence spectroscopy: spectra acquisition and spectral analysis of hydrated multilamellar liposomes

100 μl of original stock suspension was diluted up to 5 ml of phosphate buffer in order to achieve the mass concentration of DPPC ~1 mg / ml. Fluorescence spectra of the suspensions were acquired on the Agilent Cary Eclipse Spectrophotometer in the temperature range 30 – 52 °C, using 1 cm path length quartz cuvettes. The stock solutions of different DPPC + probe suspensions were diluted with 100 mM phosphate buffer, pH 7.3, to achieve 0.125 mg/mL DPPC concentration. The temperature was incrementally increased by 1°C and after 2 min

equilibration the spectra was recorded. Table 1 shows excitation wavelengths, emission bands, excitation and emission optical slits for each individual suspension sample. The fluorescence spectra of DPPC with fluorescent probes were acquired in two independent experiments.

Table 1. Settings used for the fluorescence spectra recording: λ_{Ex} – excitation wavelength, λ_{Em} – emission band, Ex slit – excitation optical slit, Em slit – emission optical slit

suspension	λ_{Ex}[a]	λ_{Em}[a]	Ex slit[a]	Em slit[a]
DPPC[b]	280	320-450	20	20
DPPC + DPA	380	400-600	5	10
DPPC + BPEA	470	480-600	5	5
DPPC + Cl-BPEA	485	500-600	5	5
DPPC + L	380	400-600	2.5	5
DPPC + R	550	560-750	2.5	5

[a] In nm; [b] In the case of liposome suspension, there was no fluorescence, the observed phenomenon is due to the dispersion.

Before venturing into multivariate curve analysis (MCA), temperature-dependent fluorescence spectra of all suspensions were prepared using Spectragryph[25]. The procedure was as follows: i) the spectra were smoothed (Savitzky-Golay with 10 points and polynom of 3rd degree), ii) certain spectral range was selected for initial analysis, iii) spectra were baseline corrected by making vertical offset so that at one same point their ordinate is set to 0, iv) spectral range was reduced in order to eliminate the spectral parts in which temperature-dependent spectral variability is negligible. In particular, the corresponding data (except for i)) are: DPPC: 320 – 450 nm (ii), 0 at 435 nm (iii), 320- 425 nm for MCA (iv); DPPC + DPA: 400 – 560 nm (ii), 0 at 600 nm (iii), 400 – 540 nm for MCA (iv); DPPC + BPA: 480 – 600 nm (ii), 0 at 600 nm (iii), 400 – 580 nm for MCA (iv); DPPC + Cl-BPEA: 500 – 600 nm (ii), 0 at 600 nm (iii), 500 -580 nm for MCA (iv); DPPC + L: 400 – 600 nm (ii), 0 at 600 nm (iii), 400 – 600 nm for MCA (iv); DPPC + R: 560 – 690 nm (ii), 0 at 690 nm (iii), 560 – 660 nm for MCA (iv).

Temperature-dependent spectra prepared in this way were further analyzed in a multivariate fashion following the protocol described previously[18]. Briefly, temperature-dependent spectra constitute data matrix (**D**) that can be separated as a product of two factors: one is spectrum of particular species (matrix of spectral profile of particular species, **S**), and another is its concentration (matrix of concentration profile of particular species, **C**):

$$\mathbf{D} = \mathbf{C}\mathbf{S}^{\mathrm{T}} + \mathbf{E}$$

E stands for residual matrix that contains unexplained data, i.e. the information not contained in **C** and **S**.

Before going into MCA, it is necessary to carefully assume the number of components that constitute the system. Since in the examined temperature range we monitor the signal of fluorescent probe the position of which in all but one system remains effectively unchanged (L undergoes conformational change due to change in lipid ordering in DPPC + L suspension)[11], one (principal) component (c_1) projects the spectra of DPPC, DPPC + DPA, DPPC + BPEA, DPPC + Cl-BPEA and DPPC + R (essentially, this represents the change in the signal intensity); accordingly, two (principal) components (c_1 and c_2) project the spectra of DPPC + L (the change in signal intensity + signal displacement). The concentration profiles (c_1 (and c_2)) display sigmoid character and their inflection points (that correspond to the phase transition(s) temperature(s)[18,26]) are obtained by fitting them on a single (T_p or T_m) or double (T_p and T_m) Boltzmann profiles, depending on the R^2 values of particular fit. Statistically most significant fit results are further discussed and are as follows: DPPC (c_1): $T_p = 35.5 \pm 0.1$ °C, $T_m = 44.6 \pm 0.7$, $R^2 = 0.997$; DPPC + DPA (c_1): $T_p = 36.4 \pm 0.1$ °C, $T_m = 54 \pm 1$, $R^2 = 0.999$; DPPC + BPEA (c_1): $T_p = 37.4 \pm 0.3$ °C, $R^2 = 0.976$; DPPC + Cl-BPEA (c_1): $T_p = 34 \pm 1$ °C, $T_m = 42.2 \pm 0.8$, $R^2 = 0.980$; DPPC + L (c_1 / c_2): $T_p = 40.7 \pm 0.5$ °C / 39.4 ± 0.7 °C, $T_m = 42.6 \pm 0.1$ / 42.6 ± 0.1 °C, $R^2 = 0.999$ / 0.999; DPPC + R (c_1): $T_p = 41.5 \pm 0.5$ °C, $T_m = 49 \pm 1$, $R^2 = 0.992$ (phase transitions temperatures are displayed in Table 1 as well).

2.3 DSC: preparation and thermal analysis of hydrated multilamelar liposomes

300 μl of original stock suspension was diluted with 2700 μl of phosphate buffer in order to achieve the mass concentration of DPPC ~ 5 mg / ml. The samples were placed in a degassing station for 15 minutes before they were transferred in the cell and measured. The calorimetric experiments were made in a microcalorimeter Nano-DSC, TA Instruments (New Castle, USA) at a scan rate of 1 °C min^{-1} and in the temperature range 10-70 °C (cell volume is 300 μl). Each sample was recorded two times in two heating − cooling cycles, whereas buffer–buffer scan was collected only once. After subtracting the buffer-buffer scan from raw data, the baseline was manually constructed and subtracted from the resultant curve. Phase transition temperatures of DPPC multilamellar liposomes (T_p and T_m) were determined from the second heating run (free from thermal history[27]) by reading both onsets ($_o$) and maxima ($_m$) of the curve.

2.4 DLS measurements

The size distribution of liposomes was determined by means of dynamic light scattering using a photon correlation spectrophotometer equipped with a 532 nm (green) laser (Zetasizer Nano ZS, Malvern Instruments, Worcestershire, UK). To avoid overestimation arising from the scattering of larger particles, the average hydrodynamic diameter (d_h) was obtained as the value at peak maximum of the volume size distribution. The reported results correspond to the average of six measurements. The data processing was done by the Zetasizer software 7.13 (Malvern Instruments). The hydrodynamic diameter of the liposomes (d_h) at 25 °C was found to be d_h ~ 1000 μm (0.5 mg / 10 ml).

3. Molecular dynamics simulations

To investigate the behavior of the chosen fluorescent probes, namely BPEA, Cl-BPEA, DPA, L and R, we performed a set of classical MD simulations, with each of the investigated probes being simulated in two different membrane environments, namely in the gel ($L_{\beta'}$) and in the fluid (L_α) phase. The simulated systems consist of DPPC bilayer and 2 % molar ratio of a specific fluorescent probe. To prepare the simulated systems, firstly the pure DPPC bilayer systems were prepared using the membrane builder module of CHARMM-GUI (http://www.charmm-gui.org/),[28-30] with it containing 192 lipid molecules, 14660 water molecules (TIP3P water model), and 25 sodium chloride species to emulate experimental conditions. CHARMM-GUI membrane builder minimization and equilibration procedure was used to obtain equilibrated simulation boxes at T = 20 °C and T = 50 °C. After aforementioned initial equilibration, both pure DPPC systems, differing in their target temperatures (T = 20 °C and T = 50 °C), were simulated for 100 ns using unbiased all-atom molecular dynamics (MD) utilizing CHARMM36m force field[31] and TIP3P water model. The final snapshots of these two simulations, representing $L_{\beta'}$ (T = 20 °C) and L_α (T = 50 °C) phases of DPPC lipid bilayer, respectively, are then used to prepare the simulations of DPPC/fluorescent probe systems. More precisely, 4 fluorescent probe molecules (consistent with the 2 % molar ratio used in the conducted experiments), being either BPEA, Cl-BPEA, DPA, L and R, are placed in the equilibrated simulation boxes of DPPC at T= 20 °C and T = 50 °C (inside the water layer). All fluorescent probes were parameterized using CHARMM36m force field.[31,24] Upon that, short pulling simulations were conducted to pull fluorescent probes inside the lipid bilayer (reaction coordinate being distance in the direction perpendicular to the membrane, i.e., z-direction, between the centre of mass of the bilayer and the centre of mass of the probe molecule, 4

reaction coordinates per system). The obtained initial configurations of 10 prepared systems (BPEA + DPPC (20 °C), Cl-BPEA + DPPC (20 °C), DPA + DPPC (20 °C), L + DPPC (20 °C) and R + DPPC (20 °C), BPEA + DPPC (50 °C), Cl-BPEA + DPPC (50 °C), DPA + DPPC (50 °C), L + DPPC (50 °C) and R + DPPC (50 °C)) are then propagated for 5 ns in the NPT ensemble, using Nosé-Hoover thermostat[32] with Berendsen barostat[33] (p = 1 bar, semiisotropic pressure coupling) to equilibrate the simulation boxes. The equilibrated boxes of 10 prepared fluorescent probe + DPPC systems are then propagated for additional 100 ns, thus constituting production runs. All simulations were performed in GROMACS 2018.4[34] with a time step of 2 fs, van der Waals and short-range Coulomb cut-offs of 12 Å, three-dimensional periodic boundary conditions, incorporating the particle mesh Ewald procedure[35]. The production simulations (both pure DPPC and fluorescent probe + DPPC systems) were propagated using Nosé-Hoover thermostat[3225] with Parrinello-Rahman barostat[36] (p = 1 bar, semiisotropic pressure coupling). The subsequent analysis is performed taking into account last 50 ns of the production simulations.

4. Results and discussion

Temperature-dependent fluorescent spectra of suspensions of DPPC in the absence and the presence of fluorescent probes are displayed in Fig. 2. In pure DPPC (due to the radiation scattering), DPPPC + BPEA, DPPC + Cl-BPEA and DPPC + R only the signal intensity changes as the temperature rises; in particular, in DPPC (Fig. 2a), DPPC + Cl-BPEA (Fig. 2d) and DPPC + R (Fig. 2f) the signal (with maximum at 376 nm, 509 nm and 524 nm, respectively) decreases with temperature increase. In temperature-dependent fluorescence spectra of DPPC + BPEA (Fig. 2c) the behavior is opposite; the signal with maximum at 509 nm increases as temperature rises. In addition to the signal intensity decrease, in temperature-dependent fluorescence spectra of DPPC + DPA the signal maxima displace from 421 nm and 439 nm at 30 °C to 412 nm and 432 nm at 52 °C (Fig. 2b). In DPPC + L (Fig. 2e) suspension the signal with maximum at 446 nm at 30 °C suddenly declines at DPPC T_m and shifts to 483 nm at 52 °C, which is due to the change in L conformation as the lipids change their ordering[1110],[37].

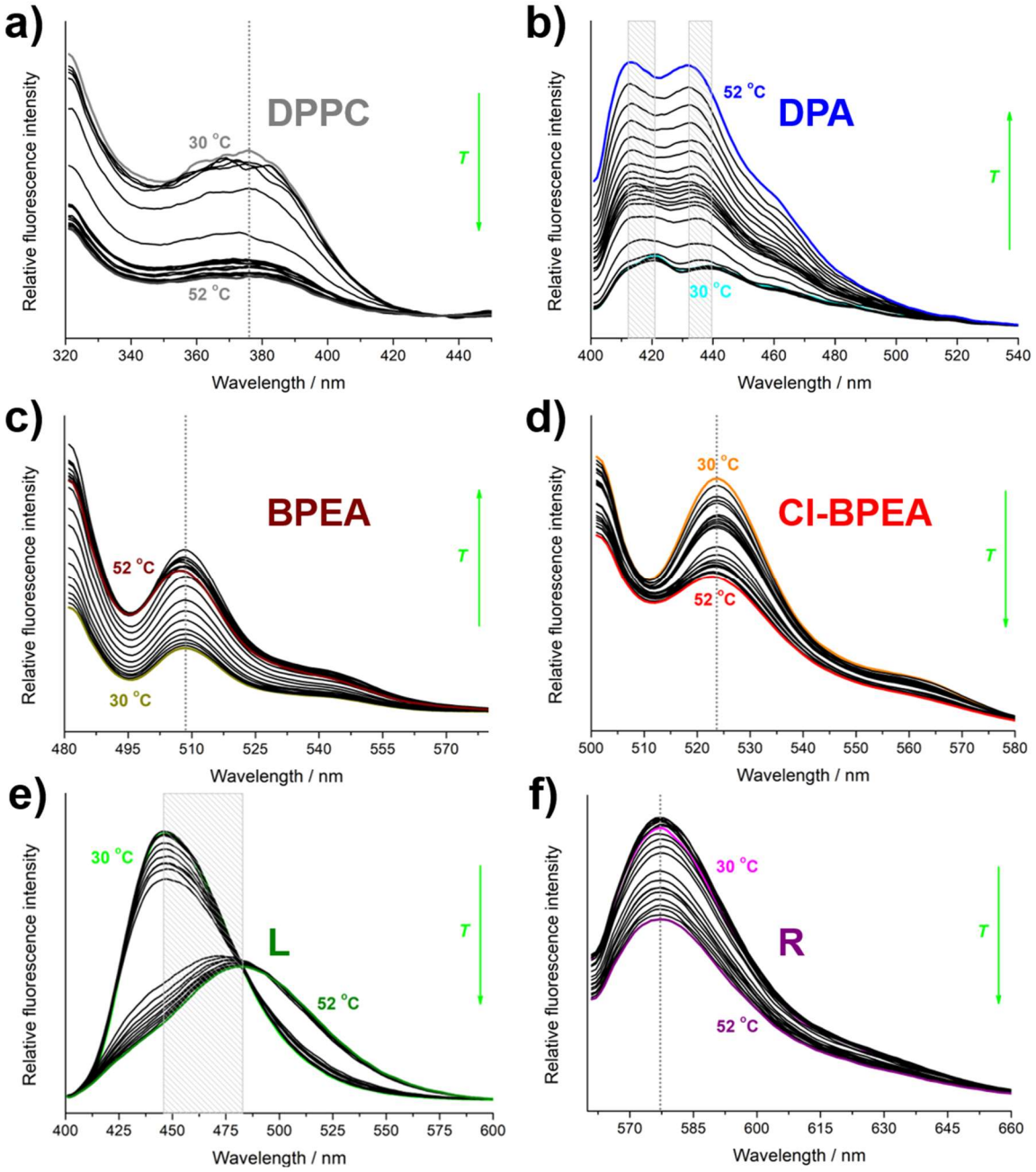

Fig. 2. Temperature-dependent fluorescence spectra of DPPC suspensions with highlighted spectra acquired at lowest (30 °C) and the highest (52 °C) temperature: a) without fluorescent probe (gray line for 30 °C, dark gray line for 52 °C), b) DPPC + DPA (cyan line for 30 °C, blue line for 52 °C); c) DPPC + BPEA (dark yellow line for 30 °C, wine line for 52 °C); d) DPPC + Cl-BPEA (orange line for 30 °C, red line for 52 °C); e) DPPC + L (green line for 30 °C, olive line for 52 °C); f) DPPC + R (magenta line for 30 °C, purple line for 52 °C). The position and eventual displacement of signal maximum/maxima are emphasized.

Phase transition temperatures (T_p and T_m) of DPPC multibilayers in the absence and in the presence of fluorescent probes are available from both multivariate analysis of temperature-dependent fluorescent spectra and from their DSC curves (Fig. 3). In general, T_p and T_m data obtained from temperature-dependent fluorescent spectra provide somewhat higher values than those obtained from DSC, which is exceptionally pronounced when compared with those determined from the transitions onsets and especially for Cl-BPEA and R (all values are displayed in Fig. 3 and in Table 2). Therefore, in the continuation of the text we will compare that values with DSC values determined from the transition maxima ($T_{p/m,\,m}$). For pure DPPC $T_{p,\,m}$ and T_p determined from DSC and temperature-dependent fluorescent spectra display excellent agreement (35.8 ± 0.1 °C and 35.5 ± 0.1 °C, respectively), while corresponding $T_{m,\,m}$ and T_m values differ for about 3 °C (41.9 ± 0.1 °C and 44.6 ± 0.7 °C, respectively). Furthermore, it seems that temperature-dependent fluorescent spectra barely register the main phase transition (Fig. 3a). Analogous values of $T_{p,\,m}$ and T_p in DPPC + DPA (Fig. 3b) suspension differ for about 1 °C (35.6 ± 0.1 °C and 36.4 ± 0.1 °C, respectively) and $T_{m,\,m}$ and T_m are actually uncomparable (41.8 ± 0.1 °C is a reasonable value unlike 54 ± 1 °C obtained as the result of a fit, respectively). Consequently, in this suspension is impossible to state whether the temperature-dependent fluorescent spectra are more sensitive to the pre- or main phase transition. In DPPC + BPEA suspension (Fig. 3c) $T_{p,\,m}$ and T_p differ for about 2 °C (35.3 ± 0.1 °C and 37.4 ± 0.3 °C, respectively), and T_p remains unregistered ($T_{m,\,m}$ is 41.8 ± 0.1 °C). The outcome of incorporation of Cl-BPEA in DPPC multibilayers (Fig. 3d) gives phase transition temperatures from DSC and temperature-dependent fluorescence measurements that coincide within the uncertainty limits ($T_{p,\,m}$ and T_p are 34.6 ± 0.1 °C and 34 ± 1 °C, and $T_{m,\,m}$ and T_m are 41.6 ± 0.1 °C and 42.2 ± 0.8 °C, respectively). Interestingly, L incorporated in DPPC multibilayers not only does it not show particular sensitivity to pretransition, but it also detects it at temperatures about 5 °C higher (40.7 ± 0.5 °C and 39.4 ± 0.7 °C) than those obtained from DSC measurements (35.1 ± 0.1 °) (Fig. 3e). The main phase transition is found to be about 1 °C higher in spectroscopic (42.6 ± 0.1 °C and 42.6 ± 0.1 °C) than calorimetric (41.8 ± 0.1 °C) measurements. Finally, monitoring the temperature-dependent fluorescence of R (Fig. 3f) one gets the lower temperature transition at 41.5 ± 0.5 °C (34.8 ± 0.1 °C from DSC) and the higher one is barely registered at 49 ± 1 °C (42.0 ± 0.1 °C from DSC).

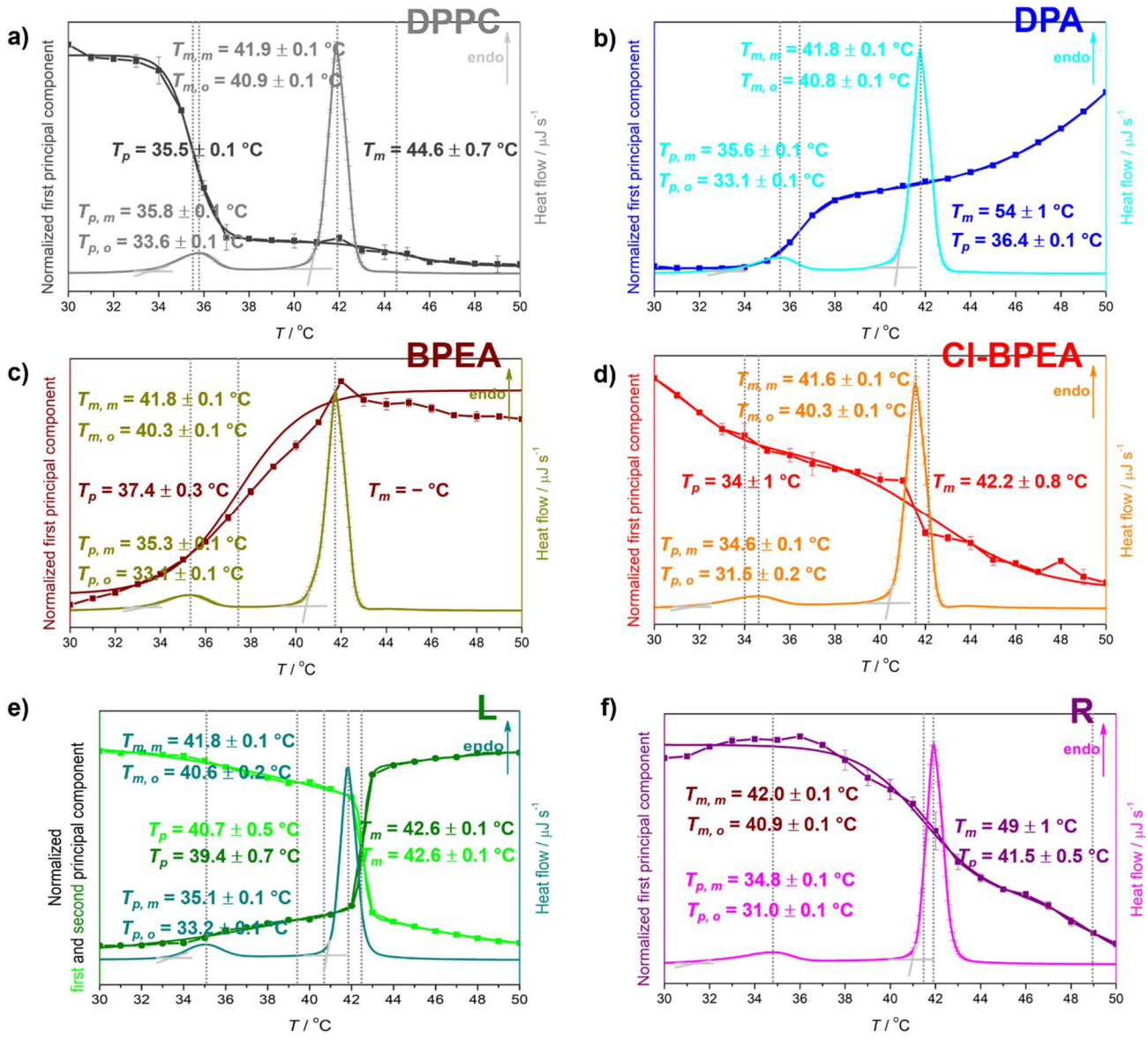

Fig. 3. Normalized first (and second in the case of L) principal component(s) of temperature-dependent fluorescence spectra, along with accompanied DSC curves of: DPPC (gray and light gray), DPPC + DPA (blue and cyan); DPPC + BPEA (wine and dark yellow); DPPC + Cl-BPEA (red and orange); DPPC + L (green and olive and dark cyan); DPPC + R (purple and magenta). Phase transition temperatures (T_p and T_m) obtained from sigmoidal fits of spectral projections and DSC curves (by reading both onsets and curve maxima) are presented on figures and are labeled with corresponding color, as well as their inflection points (dotted lines).

Table 2. Phase transition temperatures (in °C) of DPPC in the absence/presence of fluorescent probes measured by DSC (T_p and T_m determined from both onset ($_o$) and maximum ($_m$) of the

particular transition) and by MCA of temperature-dependent fluorescence spectra (FS; T_p and T_m)

suspension	T_p[a]		T_m[a]	
	DSC $T_{p,\,o\,/\,m}$	FS	DSC $T_{m,\,o\,/\,m}$	FS
DPPC	33.6 ± 0.1 / 35.8 ± 0.1	35.5 ± 0.1	40.9 ± 0.1 / 41.9 ± 0.1	44.6 ± 0.7
DPPC + DPA	33.1 ± 0.1 / 35.6 ± 0.1	36.4 ± 0.1	40.8 ± 0.1 / 41.8 ± 0.1	54 ± 1
DPPC + BPEA	35.3 ± 0.1	37.4 ± 0.3	40.3 ± 0.1 / 41.8 ± 0.1	-
DPPC + Cl-BPEA	31.5 ± 0.2 / 34.6 ± 0.1	34 ± 1	40.3 ± 0.1 / 41.6 ± 0.1	42.2 ± 0.8
DPPC + L	33.2 ± 0.1 / 35.1 ± 0.1	40.7 ± 0.5 39.4 ± 0.7	40.6 ± 0.2 / 41.8 ± 0.1	42.6 ± 0.1 42.6 ± 0.1
DPPC + R	31.0 ± 0.1 / 34.8 ± 0.1	41.5 ± 0.5	40.9 ± 0.1 / 42.0 ± 0.1	49 ± 1

[a] In °C.

We observed minor but systematic deviations in phase transition temperatures obtained from DSC and temperature-dependent fluorescence spectra. However, there are also significant differences in the probes' fluorimetric response to the particular phase transition. With pure DPPC, we detect only scattering, and the corresponding response is the largest in pretransition, while the main phase transition is barely detected (Fig. 3a). This faintly detectable main transition is found at a considerably higher temperature than expected according to DSC and literature data reported so far (44.6 ± 0.7 °C)[38]. Significantly higher sensitivity on the pretransition is observed in DPPC + DPA and DPPC + BPEA, where the fluorescence intensity increases upon heating. Furthermore, with DPPC + DPA, T_m obtained by fitting the curve on two sigmoid transitions is excessive (54 ± 1 °C, Fig. 3b), whereas for BPEA second inflection point (Fig. 3c). Cl-BPEA and L reflect both pre- and main phase transition, differing in that Cl-BPEA is equally sensitive to both pre- and main phase transition (Fig. 3d), while L is more sensitive to the main phase transition (Fig. 3e). Additionally, the curves originated from DPPC + L suspension resemble those obtained by temperature-dependent FTIR spectra of DPPC[26], in which the depth of particular sigmoid transition is proportional to the cooperativity degree of the associated phase transition. R incorporated in DPPC multibilayers does not detect any phase transition below 40 °C, making it relatively insensitive to the pretransition (Fig. 3f).

The deviation of lipid phase transitions temperatures obtained by DSC and temperature-dependent fluorescence spectroscopy might be the consequence of the fact that the

corresponding temperatures are captured indirectly, i.e. not by monitoring the behaviour of the bilayer but by observing the fluorimetric changes in the particular probe[9,10,12]. The probe's location within the bilayer and the solvation status of the probe are just two of the many factors influencing fluorescence signals. Thus, not every probe is appropriate for examining lipid thermal behaviour; for instance, the increase of fluorescence of DPA and BPEA in DPPC is not a property desirable for fluorescent probes[39]. Moreover, these probes either show an exaggerated value of the main phase transition (DPA) or do not show it at all (BPEA). The deviations observed for L, regarding both T_p and T_m, may be due to the fact that the fluorescent signal of L reflects the completion of the particular phase transition and not the beginning, which is the opposite from the data observed in temperature-dependent UV/Vis[18] and FTIR[26] spectra (Table 1). As for the R, the absence of a DPPC phase transition below 40 °C is probably due to its incorporation site.

We conducted MD simulations and calculated the number density profiles (Fig 4.) to observe the behaviour of the investigated fluorescent probes in the atomic detail. Thus, we focused on the specific positioning of the probes inside the DPPC bilayers in different states, namely $L_{\beta'}$ (T = 20 °C) and L_α (T = 50 °C) phases. It can be noticed from Fig. 4 that L exhibits by far the most significant change regarding its behaviour inside the lipid bilayer when DPPC transitions from $L_{\beta'}$ (20 °C) to L_α (50 °C) phase. More precisely, L possesses a strong peak in its number density distribution at around z = 0 at 20 °C, with its number density profile drastically changing at 50 °C, where it exhibits double peak distribution, with peaks lying approximately 1 nm from the centre of DPPC bilayer. The other fluorescent probes also exhibit changes in their profiles. Generally, the more complex number density profiles at 20 °C become relatively smooth double-peak profiles at 50 °C. However, the differences in their positioning inside the bilayer with the transition of the DPPC bilayer from $L_{\beta'}$ to its L_α phase are significantly smaller than L. This finding correlates rather well with the conducted experiments, as L showed by far the best ability to detect the main phase transition of the DPPC bilayer (see Fig. 3). On the other hand, R is showing a rather small difference in its $L_{\beta'}$ and L_α number density profiles (Fig. 4, lower panel, right, compare straight and dashed violet curves).

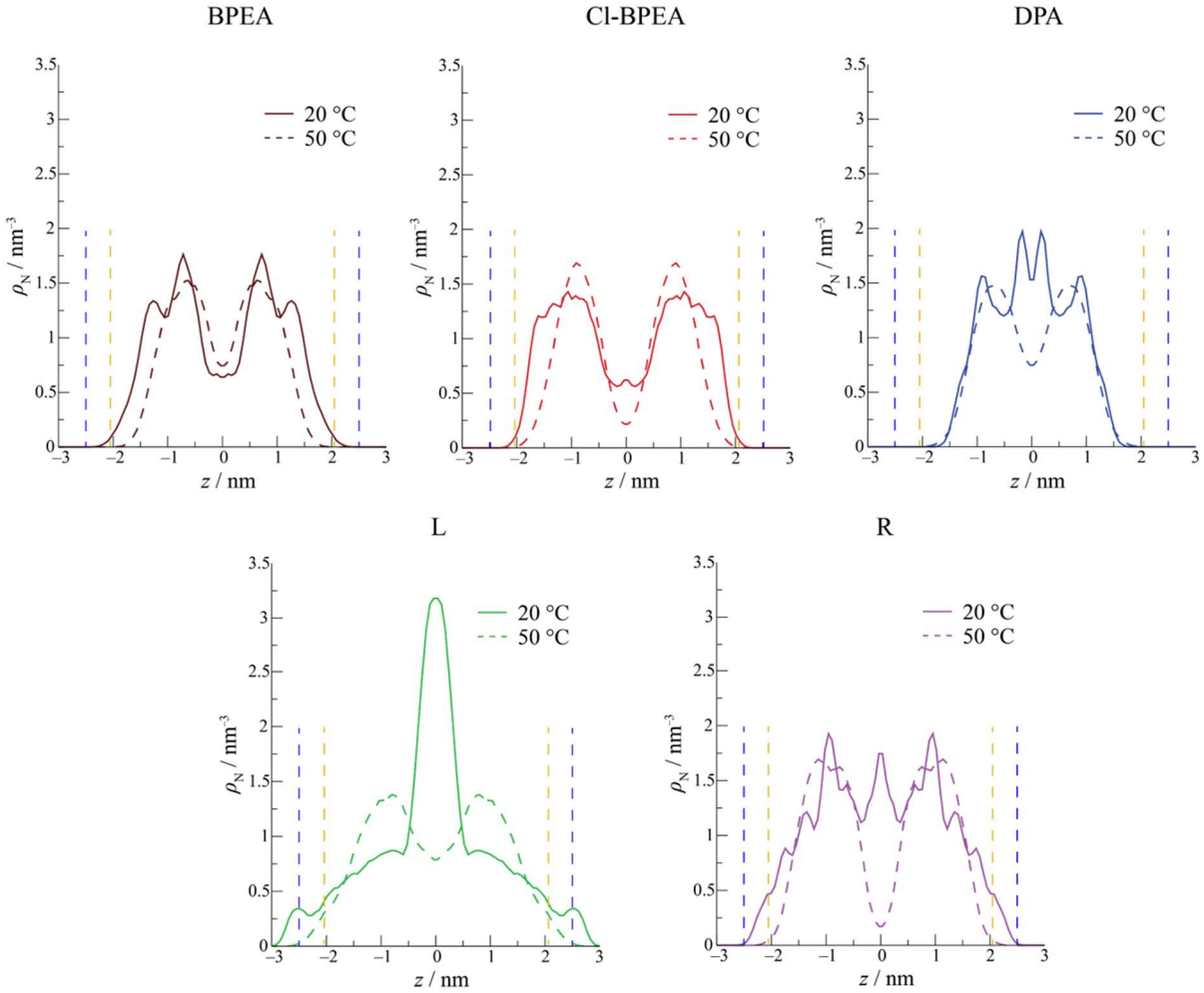

Fig. 4. Symmetrized number density profiles along the direction perpendicular to DPPC membrane (perpendicular to the *z*-direction) for all investigated fluorescent probes and both DPPC lipid states (z = 0 denotes the centre of the respective DPPC bilayer). Dashed blue and orange lines denote the distance of the centres of mass of the lower and upper leaflets (defined by the position of phosphorous atoms belonging to DPPC lipid head groups) from the bilayer centres at 20 °C and 50 °C, respectively.

Although it somewhat occupies the centre of the bilayer in its $L_{\beta'}$ phase and not in the L_α phase of the lipid, R shows similar features in both investigated cases, i.e. dominant peaks appear at around 1 nm from the centre of the DPPC bilayer at both investigated temperatures. Interestingly, DPA, L and R show the feature mentioned above, namely they occupy the central regions of the bilayer to certain extent in the DPPC $L_{\beta'}$ phase, showcasing a peak around z = 0 (peak strength trend: L > DPA > R). However, this is not the case when BPEA and Cl-BPEA are considered. Certain differences in the latter two probes can be observed in Fig. 4 (upper

panel, compare left and central subfigures), with Cl-BPEA showing higher bilayer protrusion than BPEA. Cl-BPEA resides closer to phosphate groups of DPPC, especially in the gel phase. The discrepancies between the two can also be observed from the experimental measurements (Fig. 3). Cl-BPEA can capture the pretransition of the DPPC bilayer, while BPEA is insensitive to it. Therefore, we decided to investigate these two probes in more depth. In addition to this, we also further examined the behaviour of the most potent fluorescent probe, namely L. Therefore, we present Fig. 5, highlighting the behaviour of the specific moieties present in Cl-BPEA/BPEA and L.

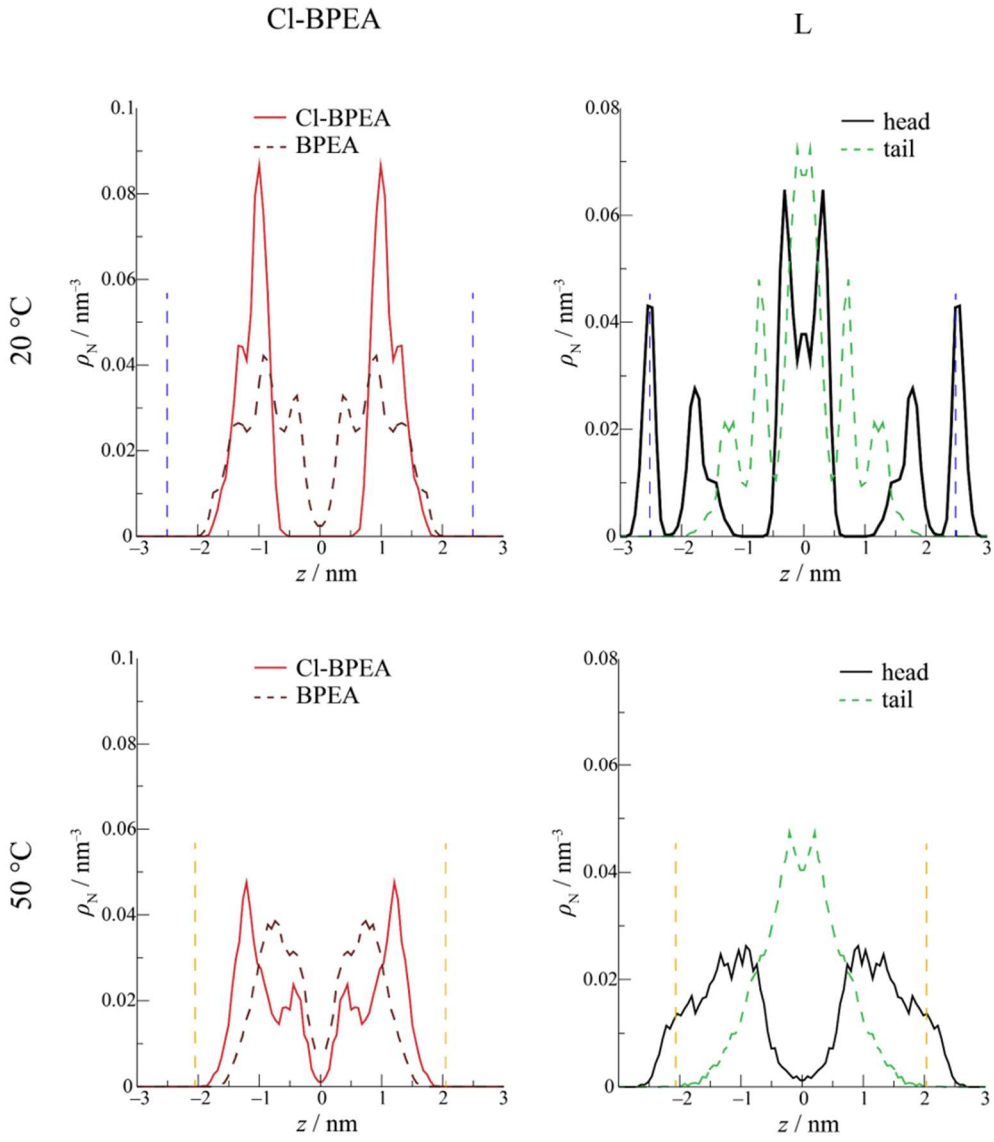

Fig. 5. Left panel: symmetrized number density profiles along the direction perpendicular to DPPC membrane (perpendicular to the *z*-direction) for chlorine atom inside Cl-BPEA (red straight line) and equivalent hydrogen atoms in BPEA (dark red dashed line). Right panel: symmetrized number density profiles along the direction perpendicular to DPPC membrane,

with black straight line denoting the head of L (nitrogen atom belonging to the head group of L), while green dashed line denotes the tail of L (C12 atom from its aliphatic tail). Dashed blue and orange lines denote the distance of the centres of mass of the lower and upper leaflets (defined by the position of phosphorous atoms belonging to DPPC lipid head groups) from the bilayer centres at 20 °C and 50 °C, respectively.

More precisely, the number density profiles of Cl-atom belonging to Cl-BPEA and the equivalent hydrogen atoms from BPEA (number density of all 4 equivalent hydrogen atoms calculated and divided by 4 to be directly comparable to Cl) are presented in the left panel. At the same time the position of the head and the tail of L are displayed in the right panel of Fig. 5. Thereby it is found that regarding the difference between Cl-BPEA and BPEA, Cl-atoms occupy region closer to the head groups of DPPC. Apart from protruding toward the outer sections of the membrane (Fig. 6, left panel), Cl-atoms are also more regiospecific than their hydrogen counterparts from BPEA. Therefore, showing narrower peaks for Cl in Cl-BPEA compared to peaks stemming from H atoms in BPEA (Fig. 5, left panel). Most strikingly, a rather minute difference in the number density profiles is observed when going from Lβ' toward the Lα phase in the case of H atoms belonging to BPEA. In contrast, Cl moiety present in Cl-BPEA shows a drastic change in the intensity of its main peaks within the same transition. Implying that its regioselectivity diminishes significantly, going from 20 °C to 50 °C. This finding could thus tentatively explain why Cl-BPEA is somewhat more sensitive toward lipid transitions compared to BPEA.

On the other hand, a stark difference in the behaviour of L can be easily observed in Fig. 5 (right panel) with respect to the same lipid transition. In the Lβ' phase, we find that L possesses a strong tendency toward populating the mid-sections of the bilayer with its tail showing some more proclivity toward populating both central sections of the bilayer, while its head group populates all sections but prefers to localise closer to the membrane/water interface. However, a different picture is obtained at 50 °C. In the fluid phase of DPPC, the head group of L exhibits significantly more homogeneous behaviour, primarily pointing toward the membrane/water interface, while the tail group again primarily occupies the inner regions of the membrane (Fig. 6, right panel). This rather significant difference in the equilibrium behaviour of L when in the $L_{\beta'}$ or L_{α} phase of DPPC can thus be considered the principal driving force making this fluorescent probe as potent as shown experimentally.

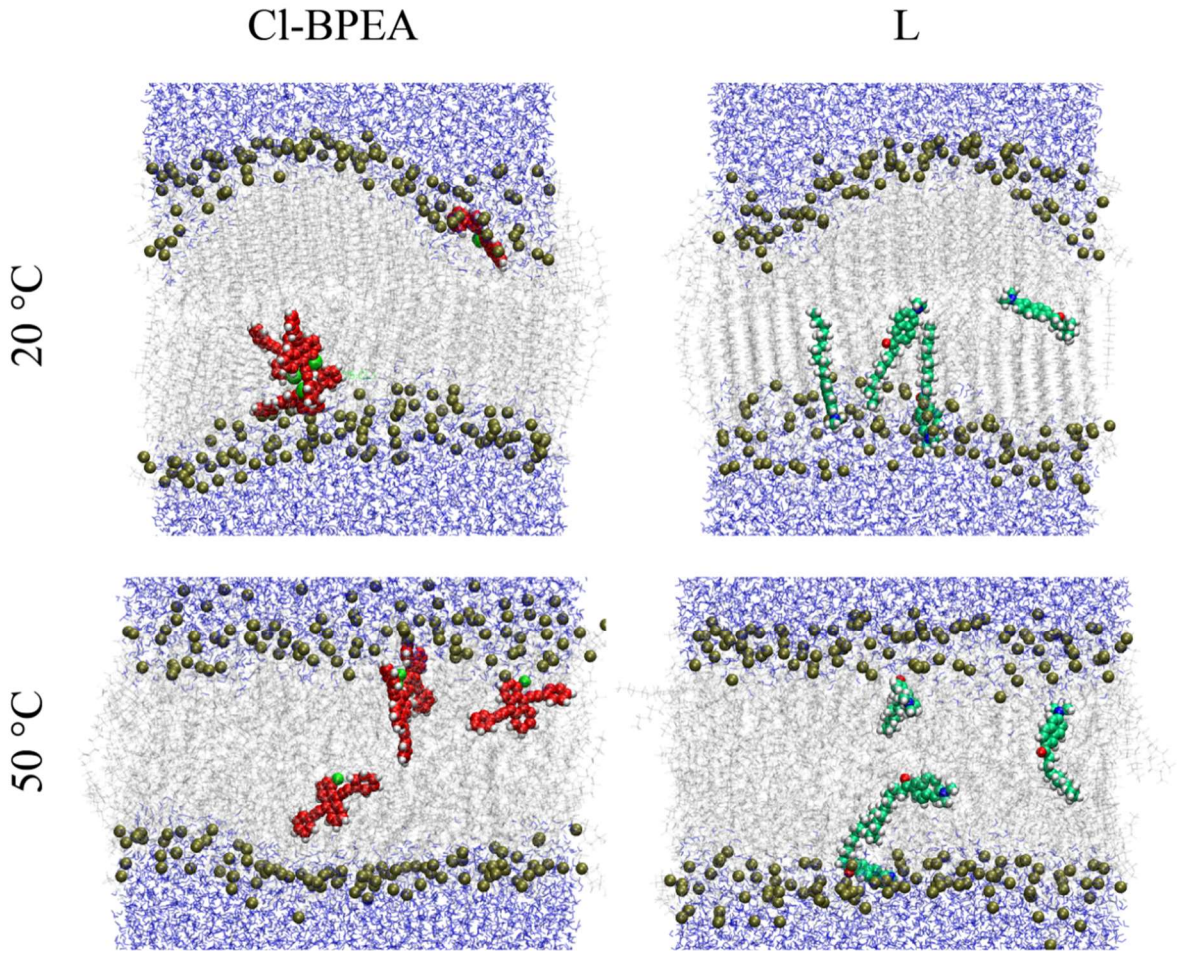

Fig. 6. Snapshots of Cl-BPEA+DPPC (left) and L+DPPC (right) in the gel (upper panel) and the fluid (lower panel) phase of DPPC bilayer. Cl-BPEA is coloured in red, with the chlorine atom shown in bright green, L is shown in dark green (its N and O atoms shown in blue and red, respectively), and phosphorous atoms belonging to lipid heads are presented in dark yellow. All aforementioned atoms are shown using vdW (spherical) representation. The remainder of the DPPC lipids is presented in light silver, while water molecules surrounding the bilayer are given in blue. Visualization: VMD software package[40]

5. Conclusion

We have examined the thermal behaviour of DPPC multibilayers in the presence of several fluorescent probes (γ = 2 %) to evaluate the possibility of detecting lipid phase transition temperatures by analyzing the shift in signals of incorporated fluorescent probes. Temperature-dependent signals of fluorescent probes were analyzed using MCA, and from obtained spectral projections, phase transition temperatures were determined. Obtained values were compared with those measured from DSC, and possible origins of their differences were discussed. The response and sensitivity of fluorescent probes are highly dependent on the position of a probe

within a lipid bilayer. Non-polar fluorescent probes buried relatively deep in the bilayer (DPA, BPEA) detect T_p with much greater sensitivity than T_m. L, the probe that stretches along the particular leaflet, detects both T_p and T_m, with the sensitivity for the latter being much higher than the former. R, located near the bilayer surface, detects phase transitions only above 40 °C. Cl-BPEA is the only probe that reflects T_p and T_m values comparable with those obtained by DSC and detects them with almost equal sensitivity. Additionally, L does not display the response at the beginning of the phase transition but its end. Overall, the fluorescence probes, namely L and Cl-BPEA can be considered as an excellent indirect tool for the determination of lipid phase transition temperatures, using readily available methodology, the temperature-dependent fluorescence spectra measurement.

Supporting Information

Supporting Information associated with this paper can be found in the online version at http://.

Acknowledgment

This paper was supported by Croatian Science Foundation, Project Project Nos. UIP-2020-02-7669 and IP-2018-01-1754. The authors gratefully acknowledge Dr. Darija Domazet Jurašin (Laboratory for Biocolloids and Surface Chemistry, Ruđer Bošković Institite) for conducting DLS measurements.

References:

[1]Komiya, M.; Kato, M.; Tadaki, D.; Ma, T.; Yamamoto, H.; Tero, R.; Tozawa, Y.; Niwano, M.; Hirano-Iwata, A. Advances in Artificial Cell Membrane Systems as a Platform for Reconstituting Ion Channels. *The Chemical Record* **2020**, *20* (7), 730–742. https://doi.org/10.1002/tcr.201900094.

[2]Köper, I. Insulating Tethered Bilayer Lipid Membranes to Study Membrane Proteins. *Mol. BioSyst.* **2007**, *3* (10), 651–657. https://doi.org/10.1039/B707168J.

[3]Bagatolli, L. A. To See or Not to See: Lateral Organization of Biological Membranes and Fluorescence Microscopy. *Biochim Biophys Acta* **2006**, *1758* (10), 1541–1556. https://doi.org/10.1016/j.bbamem.2006.05.019.

[4]Amaro, M.; Šachl, R.; Jurkiewicz, P.; Coutinho, A.; Prieto, M.; Hof, M. Time-Resolved Fluorescence in Lipid Bilayers: Selected Applications and Advantages over Steady State. *Biophys J* **2014**, *107* (12), 2751–2760. https://doi.org/10.1016/j.bpj.2014.10.058.

[5]Bouvrais, H.; Pott, T.; Bagatolli, L. A.; Ipsen, J. H.; Méléard, P. Impact of Membrane-Anchored Fluorescent Probes on the Mechanical Properties of Lipid Bilayers. *Biochimica et Biophysica Acta (BBA) - Biomembranes* **2010**, *1798* (7), 1333–1337. https://doi.org/10.1016/j.bbamem.2010.03.026.

[6]Cunningham, B. A.; Brown, A.-D.; Wolfe, D. H.; Williams, W. P.; Brain, A. Ripple Phase Formation in Phosphatidylcholine: Effect of Acyl Chain Relative Length, Position, and Unsaturation. *Phys. Rev. E* **1998**, *58* (3), 3662–3672. https://doi.org/10.1103/PhysRevE.58.3662.

[7]Heimburg, T. A Model for the Lipid Pretransition: Coupling of Ripple Formation with the Chain-Melting Transition. *Biophysical Journal* **2000**, *78* (3), 1154–1165. https://doi.org/10.1016/S0006-3495(00)76673-2.

[8]Heimburg, T. A Model for the Lipid Pretransition: Coupling of Ripple Formation with the Chain-Melting Transition. *Biophysical Journal* **2000**, *78* (3), 1154–1165. https://doi.org/10.1016/S0006-3495(00)76673-2.

[9]Langner, M.; Pruchnik, H.; Kubica, K. The Effect of the Lipid Bilayer State on Fluorescence Intensity of Fluorescein-PE in a Saturated Lipid Bilayer. *Z Naturforsch C J Biosci* **2000**, *55* (5–6), 418–424. https://doi.org/10.1515/znc-2000-5-618.

[10]Sasaki, H.; White, S. H. A Novel Fluorescent Probe That Senses the Physical State of Lipid Bilayers. *Biophys J* **2009**, *96* (11), 4631–4641. https://doi.org/10.1016/j.bpj.2009.03.003.

[11]Osella, S.; Knippenberg, S. The Influence of Lipid Membranes on Fluorescent Probes' Optical Properties. *Biochim Biophys Acta Biomembr* **2021**, *1863* (2), 183494. https://doi.org/10.1016/j.bbamem.2020.183494

[12] Deepa, H. R.; Thipperudrappa, J.; Kumar, H. M. S. Effect of Temperature on Fluorescence Quenching and Emission Characteristics of Laser Dyes. *J. Phys.: Conf. Ser.* **2020**, *1473* (1), 012046. https://doi.org/10.1088/1742-6596/1473/1/012046.

[13]Weber, G.; Farris, F. J. Synthesis and Spectral Properties of a Hydrophobic Fluorescent Probe: 6-Propionyl-2-(Dimethylamino)Naphthalene. *Biochemistry* **1979**, *18* (14), 3075–3078. https://doi.org/10.1021/bi00581a025.

[14]Owen, D. M.; Rentero, C.; Magenau, A.; Abu-Siniyeh, A.; Gaus, K. Quantitative Imaging of Membrane Lipid Order in Cells and Organisms. *Nat Protoc* **2011**, *7* (1), 24–35. https://doi.org/10.1038/nprot.2011.419.

[15]Petre, R.; Zecheru, T.; Petrea, N.; Rotariu, T. Comparative Study of Commercially Available Fluorescers versus Bis(2,4,5-Trichloro-6-Carbobutoxyphenyl) Oxalate. *Revista de Chimie -Bucharest- Original Edition-* **2016**, *12*, 2464–2468.

[16]Han, B.; Yang, Y.; Chen, J.; Tang, H.; Sun, Y.; Zhang, Z.; Wang, Z.; Li, Y.; Li, Y.; Luan, X.; Li, Q.; Ren, Z.; Zhou, X.; Cong, D.; Liu, Z.; Meng, Q.; Sun, F.; Pei, J. <p>Preparation, Characterization, and Pharmacokinetic Study of a Novel Long-Acting Targeted Paclitaxel Liposome with Antitumor Activity</P>. *IJN* **2020**, *15*, 553–571. https://doi.org/10.2147/IJN.S228715.

[17]Seddon, J. M.; Cevc, G.; Marsh, D. Calorimetric Studies of the Gel-Fluid (L.Beta.-L.Alpha.) and Lamellar-Inverted Hexagonal (L.Alpha.-HII) Phase Transitions in Dialkyl- and Diacylphosphatidylethanolamines. *Biochemistry* **1983**, *22* (5), 1280–1289. https://doi.org/10.1021/bi00274a045.

[18]Maleš, P.; Brkljača, Z.; Domazet Jurašin, D.; Bakarić, D. New Spirit of an Old Technique: Characterization of Lipid Phase Transitions via UV/Vis Spectroscopy. *Spectrochimica Acta Part A: Molecular and Biomolecular Spectroscopy* **2022**, *272*, 121013. https://doi.org/10.1016/j.saa.2022.121013.

[19]Zhi, Z.; Yang, X.; Lu, L.; Wang, X. Synthesis and Verification of 9,10-Diphenylanthracene and Its Utility as a Fluorescer in a Peroxyoxalate Chemiluminescence System. An Organic Laboratory Project Integrating Synthesis with Fluorescence and Chemiluminescence. *Chem. Educator* **2000**, *5* (4), 187–189. https://doi.org/10.1007/s00897000397a.

[20]Способ получения 9, 10-бис(фенилэтинил)антрацена и его производных - патент РФ 2054406 - Шершуков В.М.,Звягинцева Д.А. https://www.freepatent.ru/patents/2054406.

[21]9,10-Diphenylanthracene CAS#: 1499-10-1 https://www.chemicalbook.com/ProductChemicalPropertiesCB5132335_EN.htm.

[22]9,10-Bis(phenylethynyl)anthracene CAS#: 10075-85-1 https://www.chemicalbook.com/ProductChemicalPropertiesCB6692340_EN.htm

[23]1-Chloro-9,10-bis(phenylethynyl)anthracene(41105-35-5) IR Spectrum https://www.chemicalbook.com/SpectrumEN_41105-35-5_IR1.htm (accessed 2022 -03 -29).

[24] Rhodamine B CAS#: 81-88-9 https://www.chemicalbook.com/ProductChemicalPropertiesCB7485569_EN.htm (accessed 2022 -03 -29).

[25] F. Menges “Spectragryph – optical software”, Version 1.2.15, 2015, https://www.effemm2.de/spectragryph/ (accessed 2022 -03 -14).

[26]Maleš, P.; Brkljača, Z.; Crnolatac, I.; Bakarić, D. Application of MCR-ALS with EFA on FT-IR Spectra of Lipid Bilayers in the Assessment of Phase Transition Temperatures: Potential for Discernment of Coupled Events. *Colloids and Surfaces B: Biointerfaces* **2021**, *201*, 111645. https://doi.org/10.1016/j.colsurfb.2021.111645.

[27]Chen, C.; Han, D.; Cai, C.; Tang, X. An Overview of Liposome Lyophilization and Its Future Potential. *J Control Release* **2010**, *142* (3), 299–311. https://doi.org/10.1016/j.jconrel.2009.10.024.

[28]Jo, S.; Kim T.; Im, W. Automated Builder and Database of Protein/Membrane Complexes for Molecular Dynamics Simulations. *PLoS One* **2007**, *2*, e880. https://doi.org/10.1371/journal.pone.0000880

[29]Wu, E. L.; Cheng, X.; Jo, S.; Rui, H.; Song, K.C.; Dávila-Contreras, E.;Qi, y.; Lee, J.; Monje-Galvan, V.; Venable, R. M.; Klauda, J. B.; Im, W. CHARMM-GUI Membrane Builder toward realistic biological membrane simulations. *J. Comput. Chem.* **2014**, *35*, 1997–2004. https://doi.org/10.1002/jcc.23702

[30]Lee, J.; Cheng, X.; Swails, J. M.; Yeom, M. S.; Eastman, P. K.; Lemkul, J. A.; Wei, S.; Buckner, J.; Jeong, J. C.; Qi, Y.; Yo, S.; Pande, V. S.; Case, D. A.; Brooks III, C. L.; MacKerrel Jr, A. D.; Klauda, J. B.; Im, W. CHARMM-GUI Input Generator for NAMD, GROMACS, AMBER, OpenMM, and CHARMM/OpenMM Simulations Using the CHARMM36 Additive Force Field. *J. Chem. Theory Comput.* **2016**, *12*, 405–413. https://doi.org/10.1021/acs.jctc.5b00935

[31]Huang, J.; Rauscher, S.; Nawrocki, G.; Ran, T.; Feig, M.; De Groot, B. L.; Grubmüller, H.; MacKerell, A. D. CHARMM36m: an improved force field for folded and intrinsically disordered proteins. *Nat. Methods* **2016**, *14*, 71–73. https://doi.org/10.1038/nmeth.4067

[32]Nosé, S. A molecular dynamics method for simulations in the canonical ensemble. *Mol. Phys.* **1984**, *52*, 255–268. https://doi.org/10.1080/00268978400101201

[33]Berendsen, H. J. C.; Postma, J. P. M.; van Gunsteren, W. F.; DiNola, A.; Haak, J. R. Molecular dynamics with coupling to an external bath, *J. Chem. Phys.* **1984**, *81*, 3684-3690. https://doi.org/10.1063/1.448118

[34]Abraham, M. J.; Murtola, T.; Schulz, R.; Pall, S.; Smith, J. C.; Hess, B.; Lindah, E. GROMACS: High performance molecular simulations through multi-level parallelism from laptops to supercomputers. *SoftwareX* **2015**, *1–2*, 19–25. https://doi.org/10.1016/j.softx.2015.06.001

[35]Essmann, U.; Perera, L.; Berkowitz, M. L.; Darden, T.; Lee, H.; Pedersen, L. G. *J. Chem. Phys.* A smooth particle mesh Ewald method. **1995**, *103*, 8577–8593. https://doi.org/10.1063/1.470117

[36]Parrinello, M.; Rahman, A.; *J. Appl. Phys.* Polymorphic transitions in single crystals: A new molecular dynamics method. **1981**, *52*, 7182–7190.

https://doi.org/10.1063/1.328693

[37]Riske, K. A.; Barroso, R. P.; Vequi-Suplicy, C. C.; Germano, R.; Henriques, V. B.; Lamy, M. T. Lipid Bilayer Pre-Transition as the Beginning of the Melting Process. *Biochimica et Biophysica Acta (BBA) - Biomembranes* **2009**, *1788* (5), 954–963. https://doi.org/10.1016/j.bbamem.2009.01.007.

[38]Koynova, R.; Caffrey, M. Phases and Phase Transitions of the Phosphatidylcholines. *Biochim Biophys Acta* **1998**, *1376* (1), 91–145. https://doi.org/10.1016/s0304-4157(98)00006-9.

[39]Sou, K.; Chan, L. Y.; Arai, S.; Lee, C.-L. K. Highly Cooperative Fluorescence Switching of Self-Assembled Squaraine Dye at Tunable Threshold Temperatures Using Thermosensitive Nanovesicles for Optical Sensing and Imaging. *Sci Rep* **2019**, *9* (1), 17991. https://doi.org/10.1038/s41598-019-54418-1.

[40]Humphrey, W.; Dalke, A.; Schulten, K. VMD: Visual Molecular Dynamics. *J Mol Graph* **1996**, *14* (1), 33–38, 27–28. https://doi.org/10.1016/0263-7855(96)00018-5.